CO_2 Activation

DOI: 10.1002/ange.201407165

Crystallographic Snapshot of an Arrested Intermediate in the Biomimetic Activation of CO_2**

Sarah L. Ackermann, David J. Wolstenholme, Chris Frazee, Ghislain Deslongchamps, Sandra H. M. Riley, Andreas Decken, and G. Sean McGrady**

Abstract: *The design of molecular catalysts that mimic the behavior of enzymes is a topical field of activity in emerging technologies, and can lead to an improved understanding of biological systems. Herein, we report how the bulky arms of the cations in $[(n\ C_4H_9)_4N]^+[HCO_3]^-$ give rise to a host scaffold that emulates the substrate binding sites in carbonic anhydrase enzymes, affording a unique glimpse of an arrested intermediate in the base-mediated binding and activation of CO_2.*

An abundant and economical source of energy is vital to the 21st century global economy. Currently this role is filled by carbon-based fuels, which account for over 75% of total energy output.[1] Our dependence on hydrocarbons has placed an unsustainable strain on the environment, mainly through rising atmospheric CO_2 concentrations.[2] Accordingly, new materials and processes for capturing and storing or converting this thermodynamically and kinetically stable molecule are essential to maintain a balance between increasing energy demands and the need to decrease greenhouse gas emissions. Aqueous amine solutions represent the most widely implemented technology for CO_2 removal but these often suffer from low absorption rates and capacities.[2,3] Additionally, the high stability of the products requires considerable energy investment to recycle the absorbents.[1–3]

Recently, the addition of small amounts of carbonic anhydrase to these amine systems has been reported to improve significantly their CO_2 uptake, and to lower the desorption temperatures of the activated products.[4,5] This can be attributed to the metalloenzyme acting as a catalyst in the reversible hydration of CO_2 to form HCO_3^-.[5] The mechanism of this reaction has been the subject of extensive experimental and theoretical studies, and is generally understood to involve the formation of a Zn^{II}–OH^- complex that initiates nucleophilic attack on a vicinal CO_2 molecule.[6–9] The resulting Zn^{II}-bound HCO_3^- moiety is then displaced by H_2O, followed by deprotonation of the Zn^{II}–OH_2 intermediate and regeneration of the active hydroxide catalyst. A better understanding of this process has led to the design of synthetic analogues that mimic the function of carbonic anhydrase enzymes.[10]

The success of such a biomimetic approach is reflected in the growing number of zinc-based systems reported to activate CO_2 rapidly and reversibly under mild conditions.[11–14] In contrast, structural analogues that replicate the substrate binding sites of these metalloenzymes are comparatively rare. This prompted us to investigate the activation of CO_2 using tetrabutylammonium hydroxide $[(n\text{-}C_4H_9)_4N]^+[OH]^-$ (**1**) as an absorbent. This system was chosen on account of its affinity for interaction with aerial CO_2 and on the ability of tetraalkylammonium cations to form host scaffolds.[15–17] Our efforts were rewarded with the isolation and characterization of an arrested intermediate in the formation of tetrabutylammonium hydrogencarbonate $[(n\text{-}C_4H_9)_4N]^+[HCO_3]^-$ (**2**), which displays the longest C–O(H) bond detected to date in any uncoordinated hydrogencarbonate anion, and which provides new and unique insights of relevance to enzyme reaction processes.

The benchmark hydrogencarbonate salt **2** was prepared through a modified literature procedure, in which CO_2 was bubbled slowly through an aqueous solution of **1** (1.5 M) until a neutral pH value was attained.[16] This reaction proceeded rapidly and resulted in complete conversion into the desired product within 20 minutes, as confirmed by the appearance of a characteristic resonance signal at $\delta = 157.7$ ppm in the ^{13}C NMR spectrum attributable to HCO_3^-. The anhydrous salt was then obtained through azeotropic dehydration using successive aliquots of Et_2O, giving rise to a colorless powder (approximately 95% yield). Remarkably, the product was found to be thermally stable, in spite of the proclivity of tetraalkylammonium salts to undergo Hofmann elimination.[18] Differential scanning calorimetry (DSC) and thermogravimetric analysis (TGA) experiments confirmed that **2** melts at a relatively high temperature (ca. 80 °C), and subsequently decomposes between 135 and 190 °C (see Figure S1 in the Supporting Information).

Crystallization from a saturated Et_2O solution and subsequent analysis by single-crystal X-ray diffraction showed the formation of an unprecedented arrested intermediate in the base-mediated activation of CO_2, namely $[(n\text{-}C_4H_9)_4N]^+[O_2C\cdots OH]^-$ (**2′**). Figure 1a shows how the large discrepancy in the size of the ions in **2′** allows the much bulkier $[(n\text{-}C_4H_9)_4N]^+$ cations to form a hydrophobic host scaffold that encapsulates two symmetry-related $[O_2C\cdots OH]^-$ moieties. The absence of a traditional hydrogen-bond donor or acceptor on the cations lead to a head-to-tail orientation of the $[O_2C\cdots OH]^-$ anions, with the two

[*] S. L. Ackermann, Dr. D. J. Wolstenholme, C. Frazee, Dr. G. Deslongchamps, S. H. M. Riley, Dr. A. Decken, Dr. G. S. McGrady
Department of Chemistry, University of New Brunswick
P.O. Box 4400, Fredericton, N.B., E3B 5A3 (Canada)
E-mail: dwolsten@unb.ca
smcgrady@unb.ca

[**] We are grateful to the Natural Sciences and Engineering Research Council of Canada (NSERC) and for financial support of this research.

Supporting information for this article is available on the WWW under http://dx.doi.org/10.1002/anie.201407165.

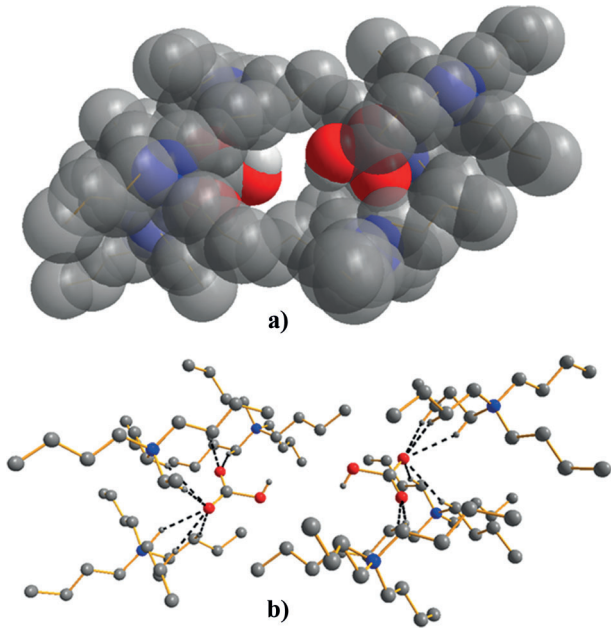

Figure 1. a) Space-filling diagram of the hydrophobic pocket in **2′** and b) the weak C–H···O interactions in this system. Geometric parameters for the interactions between ions are presented in Table S3. Atom colors: H = white, C = gray, N = blue, O = red.

hydroxy moieties separated by a long O···O distance of 4.71 Å. Notably, preliminary X-ray diffraction studies on a related solvate (**2**·THF), point to conventional dimerization of the HCO_3^- anions ($d_{O\cdots O} \approx 2.63(2)$ Å; Figure S8).[19,20]

The reorganization of the anions within the cationic host framework in **2′** leads to a significant distortion of the HCO_3^- moieties, as exemplified by the elongated C–O(H) bond length of 1.563(5) Å. This remarkable distance prompted us to perform a search of the Cambridge Structural Database (CSD), which reported 55 structures containing an HCO_3^- moiety (excluding transition-metal complexes). This survey revealed a persistent theme, with each system relying on strong hydrogen bonding between the cations/anions or a neutral organic receptor and the $[HCO_3]^-$ moieties as the primary or exclusive means of stabilizing their extended structures. In contrast, the porous nature of **2′** brings several C–H moieties into close enough proximity with the anion to facilitate unconventional C–H···O interactions ($d_{H\cdots O} = 2.29$–2.68 Å; Table S3).[21] Figure 1b shows that these contacts involve exclusively the CO_2 portion of the anions, and that their intervention helps to stabilize the structure of this arrested intermediate.

The isolation of activated HCO_3^- ions within the hydrophobic pocket in **2′** is a significant discovery, and provides an opportunity to analyze this unusual species free from any significant perturbation caused by conventional hydrogen bonding or coordination to a metal center. Based on an analysis of the Raman spectra of dilute aqueous solutions of $KHCO_3$ and $KDCO_3$, Rudolph et al. suggested that HCO_3^- monomers have C_1 symmetry.[22] Closer inspection of **2′** suggests that the $[O_2C\cdots OH]^-$ moiety also adopts this symmetry, although the size and shape of the thermal ellipsoid of the hydroxide oxygen atom indicates rotational disorder about the C–O(H) bond, preventing a definitive assignment. CCSD/6-311++G(d,p) calculations predict a planar conformation of the HCO_3^- ion, with the optimized structure lying approximately 19.1 kJ mol^{-1} lower in energy than the constrained crystallographic geometry obtained from a single-point calculation. The majority of this energy difference resides in the CO_3 portion of the HCO_3^- ion, as the barrier to rotation for the O–H bond is low ($\Delta E \approx 1.6$ kJ mol^{-1}).

The most striking outcome of this analysis is the extremely elongated C–O(H) bond length in **2′**. Figure 2 compares the

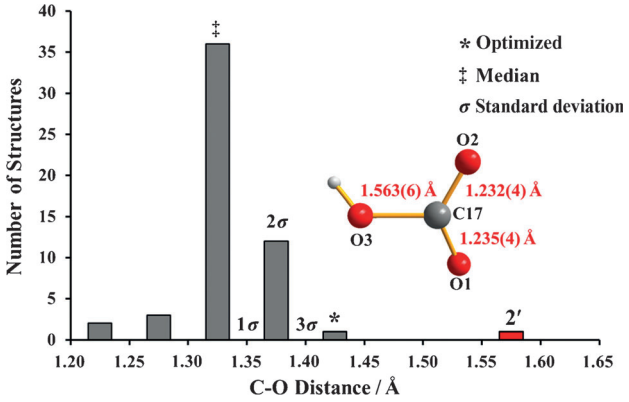

Figure 2. Distribution of C–O(H) bond lengths in all structures containing non-ligating HCO_3^- ions (72 hits from 55 structures) obtained from a survey of the CSD, along with the CCSD/6-311G(d,p) optimized HCO_3^- ion.

C···O(H) distance in the isolated anion with those obtained from the CSD search described above, which shows this moiety in **2′** to be unique: 17% longer than the average C–O(H) bond, 12% longer than the next-longest distance, and more than 3σ (three times the standard deviation) from the median C···O(H) distance. DFT calculations of the ground state HCO_3^- ion indicate a conventional C–O(H) bond length, with a vibrational stretching mode at 905 cm^{-1} and a force constant of 630 N m^{-1}. In contrast, single-point calculations constrained at the experimental C–O(H) distance for the anion in **2′** reveal a significantly weakened interaction: the vibrational frequency has decreased to 471 cm^{-1} and the force constant is lowered to a striking 130 N m^{-1}.

Widening the CSD search to include HCO_3^- ions coordinated to transition metals (50 additional structures) revealed just a single system with a longer C–O(H) bond than **2′** (Figure S7). However, this structure was poorly resolved, owing to in situ decomposition of the HCO_3^- moiety during data collection.[23] Activation of the C–O(H) bond should be accompanied by a change in the O-C-O bond angle toward a more linear orientation, rather than the 5.6° decrease detected in **2′** relative to the optimized structure of the HCO_3^- ion (Table S2). This discrepancy can be attributed to the weak C–H···O interactions present in **2′**, which draw the $[O_2C\cdots OH]^-$ ions toward the walls of the hydrophobic pocket and flatten the O-C-O portion of the ion. We conclude that the structure of the anion in **2′** represents a unique exper-

imental snapshot of the incipient binding of CO_2 by the hydroxide ion, which is both assisted and restrained by unconventional hydrogen-bonding interactions with the hydrophobic cavity formed by the tetraalkylammonium cation scaffold.

The arrested intermediate **2′** affords us fundamental insights into the base-mediated activation of CO_2, with the hydrophobic pockets in this system closely resembling the substrate binding sites of human carbonic anhydrase II (CAII).[6–9,24,25] This feature is exemplified by the C–H···O interactions that tether the HCO_3^- moieties to the walls of the host scaffold in **2′**, in which the C···O contacts are comparable to the van der Waals interactions responsible for binding CO_2 in the metalloenzyme (Table 1; Figure 3). This close analogy provides compelling evidence that the cation scaffold in **2′** plays a similar role in activating CO_2 as do the hydrophobic pockets of CAII, namely orienting the substrate to optimize its interaction with the hydroxide moiety.[6] However, the presence of a Zn^{II} cation in CAII drives the reaction through to completion and stabilizes the HCO_3^- moiety, whereas the absence of any assistance from a metal center in **2′** leaves the $[O_2C\cdots OH]^-/HCO_3^-$ equilibrium in favor of the arrested intermediate. This behavior is typical of proteins containing hydrophobic regions, in which the local pK_a value of their amino acid residues can be increased significantly on account of a more neutral local environment.[26,27] The close proximity of HCO_3^- ions in **2′** to the walls of the biomimetic hydrophobic pocket created by the tetraalkylammonium cations will result in a similar increase in the local pK_a value of this system, leading to a destabilization of the charge distribution and resulting in the observed $[O_2C\cdots OH]^-$ configuration. Remarkably, the C–O(H) bond in **2′** is 14% longer than its counterpart in CAII·$HCO_3^{<M->}$, whereas the O-C-O bond angles in these systems are nearly identical ($\Delta\sphericalangle_{O\text{-}C\text{-}O} = 6.4°$). These findings suggest that the $[O_2C\cdots OH]^-$ moiety in **2′** can justifiably be considered as a model of the initial stages of this enzymatic process, as shown in Figure 3.

To understand in more detail the unique behavior exhibited by the HCO_3^- moieties in **2′**, we carried out a series of calculations (CCSD) at various stages in the formation of this ion through the nucleophilic attack of the hydroxide anion on CO_2. This study revealed subtle details regarding the reaction coordinate using the concepts espoused in the quantum theory of "atoms in molecules" (AIM).[28] AIM theory states that the nuclei of two interacting

Table 1: Selected bond lengths for the intermolecular interactions in **1′** and the *holo* form of human carbonic anhydrase II (CAII) with a bound CO_2 molecule.[25]

2′		CAII	
Interaction	Distance [Å]	Interaction	Distance [Å]
C13···O1	3.217(4)	His94(Cε1)···O1	3.3
C1···O2	3.339(4)	Leu198(Cα)···O2	3.4
C5···O2	3.369(4)	His119(Cβ)···O1	3.5
C14···O1	3.400(5)	Val121(Cγ2)···O1	3.5
C1···O2	3.463(4)	Trp209(Cγ2)···O2	3.5
C10···O2	3.563(5)	His119(Cγ1)···O1	3.7
C3···O2	3.522(4)	Leu198(Cδ2)···O2	3.7
C9···O1	3.638(4)	Val143(Cγ1)···O1	3.7

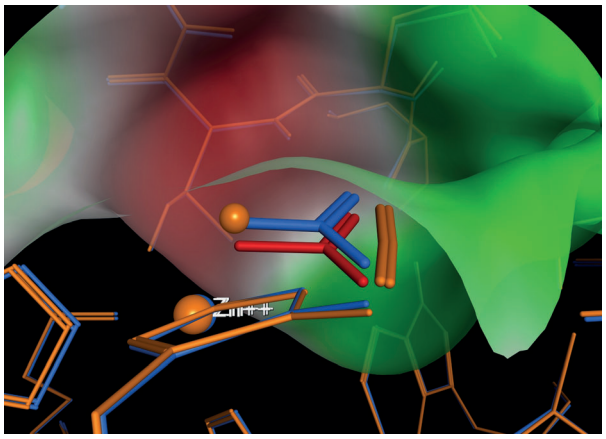

Figure 3. Plot of the active site in CAII·CO_2 (orange) superimposed on its CAII·HCO_3 (blue) counterpart, along with the structure of the $[O_2C\cdots OH]^-$ ion from **2′** (red) oriented parallel and slightly below the $[HCO_3]^-/H_2O\cdots CO_2$ plane. The zinc cations as well as the oxygen of the active-site water in CAII·CO_2 are shown as orange spheres. The green and red isosurfaces correspond to the hydrophobic and hydrophilic regions of the active site, respectively. The Figure was created using MOE 2013.08 (Chemical Computing Group Inc.).

atoms are linked by a maximum line of electron density, commonly referred to as a bond path (BP). This topological parameter is accompanied by a bond critical point (BCP), which represents the minimum in the electron density along this pathway, and a maximum in the two directions perpendicular to the tangent of the BP. This stationary point on the interatomic surface is often considered as a gateway between two atoms, and contains several features often used to characterize the nature of chemical bonds, such as the accumulation of electron density, $\rho_b(r)$, and its Laplacian, $L(r) = -\nabla^2\rho_b(r)$.

The AIM analysis reveals that a moderately strong electrostatic interaction between the two participants is established in advance of any significant activation of the CO_2 molecule ($\rho_b(r) = 0.062$ e Å^{-3} at 3.00 Å), as shown in Figure 4a. This is followed by a gradual accumulation of electron density along the $O_2C\cdots OH^-$ directrix, as the negative charge becomes redistributed between the hydroxide and CO_2 regions of the anion. This process accounts for approximately 60% of the density accumulated in the final C–O(H) bond of the optimized structure, with the balance developing rapidly between 1.43 and 1.70 Å. Notably, the $\rho_b(r)$ value for the C–O(H) bond obtained from the single-point calculation of the fixed crystallographic geometry in **2′** ($\rho_b(r) = 1.302$ e Å^{-3} at 1.56 Å), accounts for only circa 78% of the total density in its optimized counterpart. This is in full agreement with the conclusions drawn from the structural analysis, namely that **2′** can be considered as an arrested intermediate at an early stage on the reaction coordinate to formation of the HCO_3^- moiety in **2**.

The $\rho_b(r)$ values for the $O_2C\cdots OH^-$ interaction reveal three distinct stages: a) formation of an initial electrostatic interaction between the participants, b) redistribution of charge between the OH^- and CO_2 moieties, and c) the strengthening and completion of the C–O(H) bond. How-

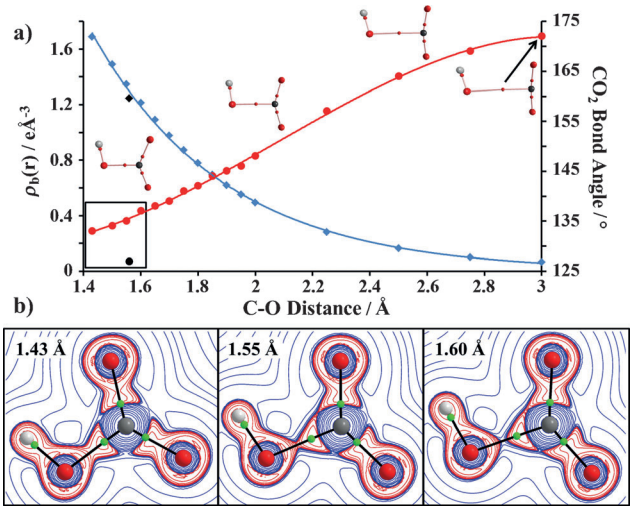

Figure 4. a) Plots of the accumulation of electron density ($\rho_b(r)$) along the $O_2C\cdots OH^-$ directrix at the BCP for the $O_2C\cdots OH^-$ interaction (blue) and the CO_2 bond angle (red) at various stages in the formation of the HCO_3^- ion. The black diamond and black sphere correspond to the values obtained from the single-point calculation for the fixed crystallographic geometry. b) Selected $\nabla^2\rho_b(r)$ plots illustrating individual steps in the formation of a covalent C–O(H) bond in HCO_3^-. The positive (blue) and negative (red) contours are plotted in increments of 2.4×10^{-2}, 4.8×10^{n}, 9.6×10^{n}, and $1.9\times10^{n+1}$ (n = −2, −1, 0, 1, 2, and 3).

ever, the $\rho_b(r)$ values provide no information about the evolution from a closed-shell (intermolecular) to a covalent (intramolecular) bonding interaction. More informative in this regard are the $\nabla^2\rho_b(r)$ values, which measure regions of charge depletion ($\nabla^2\rho_b(r) > 0$) and concentration ($\nabla^2\rho_b(r) < 0$) within a molecule, and hence provide both qualitative and quantitative metrics for the nature of chemical bonding. The $\nabla^2\rho_b(r)$ values indicate that the onset of a covalent C–O(H) bond occurs at approximately 1.70 Å (Table S5), significantly longer than the sum of the covalent radii for carbon and oxygen (ca. 1.42 Å).[29] This apparent discrepancy is a result of significant polarization of the CO_2 moiety, for which the BCP for the $O_2C\cdots OH^-$ interaction shifts into a region of local charge concentration directly adjacent to the electrophilic carbon center, leading to a negative $\nabla^2\rho_b(r)$ value that does not reflect the formation of a true covalent bond (see Supporting Information). Indeed, the $\nabla^2\rho_b(r)$ contour plots shown in Figure 4b indicate that this process actually occurs closer to our experimental geometry (ca. 1.55 Å). We conclude that the HCO_3^- moiety in **2′** represents a unique crystallographic snapshot in the formation of this anion, captured at the cusp of the transition from a closed-shell intermolecular interaction to a covalent bond.

In summary, this study has employed a biomimetic approach to isolate a rare arrested intermediate in the base-mediated activation of CO_2 using the hydroxide absorbent **1**. Subsequent characterization of the resulting product $[(n\text{-}C_4H_9)_4N]^+[O_2C\cdots OH]^-$ **2′** has afforded a unique glimpse of the early stages in the formation the HCO_3^- ion, which is captured here at the incipient formation of the covalent C–O(H) bond. This study was augmented with a CSD survey that revealed the unique nature of **2′**, which prompted a theoretical analysis of the interaction between CO_2 and OH^- ions. This analysis revealed three stages in the formation of a HCO_3^- ion: a) establishment of an electrostatic interaction, b) redistribution of charge between OH^- and CO_2, and c) the formation of a covalent C–O(H) bond. Overall, this combined experimental and theoretical approach has reproduced and characterized a binding site for CO_2 that closely resembles the hydrophobic pocket common to all CA enzymes, and has allowed us to measure in detail for the first time aspects of the nature of the binding sites of these biological catalysts, decoupled from the presence of the catalytic metal center. We anticipate that future attempts to mimic the behavior of CA enzymes will seek to incorporate a binding pocket of the form reported herein for **2′** along with the active metal site, and will lead to enhanced control and activity of this fundamental chemical process.

Received: July 13, 2014
Revised: October 1, 2014
Published online: November 5, 2014

Keywords: biomimetic system · carbon dioxide · carbonic anhydrases · electronic structure · enzyme models

[1] Y. Liu, Z. U. Wang, H.-C. Zhou, *Greenhouse Gases: Sci. Technol.* **2012**, *2*, 239 – 259.
[2] D. M. D'Alessandro, B. Smit, J. R. Long, *Angew. Chem. Int. Ed.* **2010**, *49*, 6058 – 6082; *Angew. Chem.* **2010**, *122*, 6194 – 6219.
[3] G. Puxty, R. Rowland, A. Allport, Q. Yang, M. Brown, R. Burns, M. Maeder, M. Attalla, *Environ. Sci. Technol.* **2009**, *43*, 6427 – 6433.
[4] C. K. Savile, J. J. Lalonde, *Curr. Opin. Biotechnol.* **2011**, *22*, 818 – 823.
[5] M. Vinoba, M. Bhagiyalakshmi, A. N. Grace, D. H. Kim, Y. Yoon, S. C. Nam, I. H. Baek, S. K. Jeong, *J. Phys. Chem. B* **2013**, *117*, 5683 – 5690.
[6] D. W. Christianson, C. A. Fierke, *Acc. Chem. Res.* **1996**, *29*, 331 – 339.
[7] K. M. Merz Jr., L. Banci, *J. Am. Chem. Soc.* **1997**, *119*, 863 – 871.
[8] S. Thoms, *J. Theor. Biol.* **2002**, *215*, 399 – 404.
[9] A. S. Lipton, R. W. Heck, P. D. Ellis, *J. Am. Chem. Soc.* **2004**, *126*, 4735 – 4739.
[10] G. Parkin, *Chem. Rev.* **2004**, *104*, 699 – 767.
[11] X. Zhang, R. van Eldik, *Inorg. Chem.* **1995**, *34*, 5606 – 5614.
[12] L. Koziol, C. A. Valdez, S. E. Baker, E. Y. Lau, W. C. Floyd III, S. E. Wong, J. H. Satcher Jr., F. C. Lightstone, R. D. Aines, *Inorg. Chem.* **2012**, *51*, 6803 – 6812.
[13] W. Sattler, G. Parkin, *Chem. Sci.* **2012**, *3*, 2015 – 2019.
[14] A. M. Appel, J. E. Bercaw, A. B. Bocarsly, H. Dobbek, D. L. DuBois, M. Dupuis, J. G. Ferry, E. Fujita, R. Hille, P. J. A. Kenis, C. A. Kerfeld, R. H. Morris, C. H. F. Peden, A. R. Portis, S. W. Ragsdale, T. B. Rauchfuss, J. N. H. Reek, L. C. Seefeldt, R. K. Thauer, G. L. Waldrop, *Chem. Rev.* **2013**, *113*, 6621 – 6658.
[15] I. Ravikumar, P. Ghosh, *Chem. Commun.* **2010**, *46*, 1082 – 1084.
[16] S. Dalapati, S. Jana, R. Saha, M. A. Alam, N. Guchhait, *Org. Lett.* **2012**, *14*, 3244 – 3247.
[17] M. R. J. Elsegood, *Acta Crystallogr. Sect. E* **2011**, *67*, o2599.
[18] S. Chempath, J. M. Boncella, L. R. Pratt, N. Henson, B. S. Pivovar, *J. Phys. Chem. C* **2010**, *114*, 11977 – 11983.
[19] G. A. Jeffrey, *An Introduction to Hydrogen Bonding*, Oxford University Press, Oxford, UK, **1997**.

[20] P. D. C. Dietzel, M. Jansen, *Acta Crystallogr. Sect. E* **2002**, *58*, o1003.
[21] G. R. Desiraju, T. Steiner, *The Weak Hydrogen Bond in Structural Chemistry and Biology*, Oxford University Press, Chichester, UK, **1999**.
[22] W. W. Rudolph, G. Irmer, E. Königsberger, *Dalton Trans.* **2008**, 900 – 908.
[23] F. Bottomley, J. Chen, *Organometallics* **1992**, *11*, 3404 – 3411.
[24] J. F. Domsic, B. S. Avvaru, C. U. Kim, S. M. Gruner, M. Agbandje-McKenna, D. N. Silverman, R. McKenna, *J. Biol. Chem.* **2008**, *283*, 30766 – 30771.
[25] B. Sjöblom, M. Polentarutti, K. Djinović-Carugo, *Proc. Natl. Acad. Sci. USA* **2009**, *106*, 10609 – 10613.
[26] D. G. Isom, C. A. Castañeda, B. R. Cannon, P. R. Velu, B. E. García-Moreno, *Proc. Natl. Acad. Sci. USA* **2010**, *107*, 16096 – 16100.
[27] D. G. Isom, C. A. Castañeda, B. R. Cannon, B. E. García-Moreno, *Proc. Natl. Acad. Sci. USA* **2011**, *108*, 5260 – 5265.
[28] R. F. W. Bader, *Atoms in Molecules: A Quantum Theory*, Oxford University Press, Oxford, UK, **1990**.
[29] B. Cordero, V. Gómez, A. E. Platero-Prats, M. Revés, J. Echeverría, E. Cremades, F. Barragán, S. Alvarez, *Dalton Trans.* **2008**, 2832 – 2838.

